ELSEVIER

Catalysis Today 39 (1997) 77–87

CATALYSIS TODAY

Hydrogenation of tetralin over sulfided nickel–tungstate/alumina and nickel–molybdate/alumina catalysts

H. Yasuda[a], M. Higo[b], S. Yoshitomi[b], T. Sato[a], M. Imamura[a], H. Matsubayashi[a], H. Shimada[a], A. Nishijima[a], Y. Yoshimura[a,*]

[a] *National Institute of Materials and Chemical Research, Tsukuba 305, Japan*
[b] *Shibaura Institute of Technology, Shibaura, Tokyo 108, Japan*

Abstract

Nickel–tungstate/alumina (NiW/Al_2O_3) and nickel–molybdate/alumina ($NiMo/Al_2O_3$) catalysts were prepared using an incipient wetness impregnation method with citric acid as a complexing agent. The hydrogenation activity of both sulfided catalysts was measured in a continuous-flow reactor as well as in a batch tube-bomb reactor with tetralin as an aromatic compound. Activity and stability of both sulfided catalysts were then compared in detail. The hydrogenation activity of the two catalysts depended on the partial pressure of the hydrogen sulfide (H_2S) in the reaction atmosphere, where dimethyl disulfide (DMDS) was added to control its pressure. The sulfided NiW/Al_2O_3 catalyst was advantageous in hydrogenating tetralin under low H_2S partial pressure, and the structure of the sulfide phases was quite stable in the reducing atmosphere which was measured by XPS and EXAFS methods. On the other hand, the sulfided $NiMo/Al_2O_3$ catalyst was advantageous in hydrogenating tetralin under high H_2S partial pressure, where the hydrogenation activity of both catalysts were inhibited by H_2S. The sulfided $NiMo/Al_2O_3$ catalyst under low H_2S partial pressure was less stable than the sulfided NiW/Al_2O_3 catalyst due to structural changes of the active phases, such as migration of the Ni species into γ-Al_2O_3 to form the $NiAl_2O_4$ phase and sintering of the MoS_2-like phase as confirmed by an XPS and an EXAFS. The superiority of the sulfided NiW/Al_2O_3 catalyst over the sulfided $NiMo/Al_2O_3$ catalyst was indicated in deep hydrogenation of low-sulfur feedstocks. © 1997 Elsevier Science B.V.

Keywords: Nickel–tungstate catalyst; Nickel–molybdate catalyst; Aromatic hydrogenation; TPR; XPS; EXAFS

1. Introduction

The current trend in environmental regulations of diesel emissions focuses on diesel fuel specifications, and in particular, on low levels of sulfur and aromatics and on high cetane number. For decreasing the aromatic level, two kinds of catalysts are currently used: conventional sulfide catalysts, such as NiMo and NiW, and sulfur-tolerant noble-metal catalysts. For achieving deep aromatic saturation, one option is that conventional sulfide catalysts could be used in a single-stage mode under high severity conditions taking into account the thermodynamical limitation of aromatic saturation. Another option is using conventional catalysts in the first stage of an integrated two-stage mode and using sulfur tolerant noble-metal catalysts in the second stage. In this option, conventional catalysts

*Corresponding author.

PII S0920-5861(97)00090-4

might have a moderate-level hydrogenation activity, but should keep the sulfur level of hydrotreated oils low due to the limitation of the allowable sulfur levels for the sulfur-tolerant noble-metal catalyst. Therefore, depending on the tolerable sulfur levels of noble-metal catalysts and on hydrodesulfurization (HDS) activity of conventional catalysts, feedstocks containing low amounts of sulfur can be hydrotreated over conventional sulfide catalysts.

Nickel–tungstate/alumina (NiW/Al_2O_3) catalysts are highly active in the hydrotreating and hydrocracking of middle distillates and in the upgrading of coal-derived oils, which have a low sulfur concentration [1]. These catalysts are superior to nickel–molybdate/alumina catalysts ($NiMo/Al_2O_3$) in hydrogenating a petroleum feedstock containing a low sulfur concentration, but inferior in hydrotreating a petroleum feedstock that has a high sulfur concentration [2,3]. This suggests that activity and stability of sulfided NiW/Al_2O_3 and $NiMo/Al_2O_3$ catalysts depend on the partial pressure of hydrogen sulfide (hereafter designated as $P(H_2S)$) in the reaction atmosphere. Comparing the performance of these catalysts in detail, however, is difficult because these catalysts often differ in support properties, ingredients, and preparation methods.

To compare the catalytic performance and the stability of these catalysts, in this study we used an incipient wetness impregnation method to prepare NiW/Al_2O_3 and $NiMo/Al_2O_3$ catalysts (hereafter designated as NiW and NiMo, respectively). In all cases we used a γ-Al_2O_3 support and used citric acid as a complexing agent in the impregnating solutions [4]. We then determined the W and Mo structure of the sulfided NiW and NiMo catalysts by using extended X-ray absorption fine structure (EXAFS) analysis and X-ray photoelectron spectroscopy (XPS). We then characterized these sulfided catalysts by using a temperature-programmed reduction (TPR) method. Finally, we investigated the effects of $P(H_2S)$ on the hydrogenation activity (HYG) of these catalysts by using a continuous-flow reactor with tetralin as an aromatic compound. DMDS was added to the feedstocks to control $P(H_2S)$. The inhibitory and promoting effects of H_2S on the HYG and the stability of the active phases were also investigated in a tube-bomb batch reactor with a partially reduced sulfided catalysts. The superiority of the sulfided NiW/Al_2O_3 catalyst over the sulfided $NiMo/Al_2O_3$ catalyst was indicated in the HYG and the stability of the active phases.

2. Experimental

Using an incipient wetness impregnation method, we prepared the NiW catalyst using an aqueous citrate solution of ammonium tungstate $(NH_4)_6H_2W_{12}O_{40}\cdot nH_2O$, nickel carbonate, and citric acid (at a citric acid : Ni molar ratio of 1.0). We prepared the NiMo catalyst by using an aqueous citrate solution of molybdenum trioxide, nickel carbonate, and citric acid (citric acid : Ni molar ratio of 1.2). For reference, we prepared Ni, W and Mo catalysts, again by using an aqueous citrate solution of nickel carbonate and citric acid(citric acids : Ni molar ratio of 1.2), an aqueous citrate solution of ammonium tungstate and citric acid(citric acid : W molar ratio of 0.3), and an aqueous citrate solution of molybdenum trioxide and citric acid(citric acid : Mo molar ratio of 1.1), respectively. The γ-Al_2O_3 for the supports was supplied by Catalysts and Chemicals Industries, and had a surface area of 209 m^2/g and a pore volume of 0.81 cm^3/g. The impregnated catalysts were dried at 393 K for 4 h and then calcined at 773 K for 3 h in dry air (air flow rate of 3 l/min). The amount of active components for the NiW catalyst were 4.4 wt% NiO and 30.6 wt% WO_3; for the NiMo catalyst, 4.3 wt% NiO and 16.6 wt% MoO_3; for the Ni catalyst, 4.4 wt% NiO; and for the W catalyst, 30.6 wt% WO_3. These calcined catalysts were then sulfided at 673 K with an $H_2S(5\%)/H_2(95\%)$ gas for 2 h prior to characterization and catalytic test reactions for evaluating the HYG. For the XPS and EXAFS analyses, a portion of the NiW catalysts were sulfided at 773 K for 2 h. For evaluating the HYG in the batch runs (described in Section 3.3), a portion of these sulfided catalysts were subsequently reduced under H_2 flow for 2 h at either 473 K, 673 K, and 773 K. The sulfur content of each catalyst was measured using a sulfur analyzer (LECO-SC132).

The EXAFS measurements of the sulfided catalysts (at the beam lines of BL 10B and 7C) were done at the Photon Factory of the National Laboratory for High Energy Physics (Tsukuba, Japan). Details

of the measurements are described elsewhere [5]. The XPS measurements were done on pulverized samples of the catalysts (particle diameter range of 74–149 μm) using an XPS (PHI-5400MC).

In the TPR measurements, a portion of the sulfided catalysts (0.3 g) was packed in a quartz reactor, and reduced using an H_2(50%)/N_2(50%) reducing gas, where the temperature was increased to 1073 K at a heating rate of 5 K/min and at a flow rate of 0.4 l(NTP)/min. The composition of the product gases was monitored using a mass spectrometer.

The hydrogenation of tetralin over the NiW and NiMo catalysts was carried out in a high-pressure fixed-bed continuous-flow reactor operated in the up-flow mode. The reactor was a 316 stainless steel tube (1/6 in. i.d. and 0.6 m long) and was covered with a bronze isothermal jacket whose temperature was controlled by an electric furnace. The top part of the catalyst bed (catalyst particle size of 22–48 mesh) was in contact with a thermo well (1/8 in. o.d.) 316 stainless steel) so that the reaction temperature could be measured with a thermocouple. The bottom part of the catalyst bed was filled with stainless steel beads (2 mm diameter), which acted as a preheating zone. The H_2 flow rate was controlled by a mass flow controller. The feed was supplied by a liquid chromatographic pump at a rate that was monitored using an electric balance on which a feed tank was placed. The experimental conditions were a total pressure of 3.9 MPa, reaction temperature of 573 K, weight hourly space velocity (WHSV) of 2, 4, or 6 h^{-1}, and ratio of H_2 flow rate to feed flowrate of 500 l(NTP)/l. The feed contained tetralin (30 wt%) and *n*-hexadecane (70 wt%). Dimethyl disulfide (DMDS) was added to control the pressure of H_2S (DMDS decomposition temperature of around 473 K). The liquid products of the reaction were analyzed using a gas chromatograph with a capillary column (Hewlett-Packard Ultra 1). The H_2S concentration in the product gas was analyzed using a gas chromatograph with a packed column(Gaskuropack 54).

The HYG of the sulfided–reduced catalysts were measured in a tube-bomb batch reactor (volume capacity of 50 cm^3) at 573 K under an initial H_2 pressure of 3.0 MPa for 1 h with the same type of feedstock used in the continuous-flow runs, but with no DMDS added.

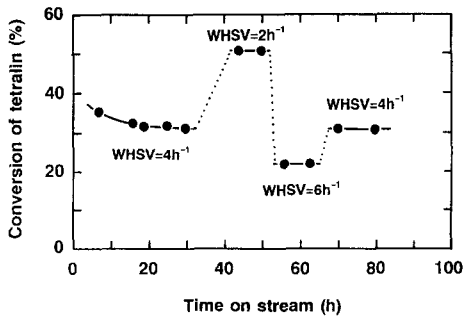

Fig. 1. Changes in hydrogenation activity of the NiW/Al_2O_3 catalysts with time on stream: 0.1 wt% of dimethyl disulfide was added as a spiking agent.

3. Results and discussion

3.1. Reaction kinetics

Fig. 1 shows the changes in the conversion of tetralin with WHSV for the sulfided (673 K) NiW catalyst at a total pressure of 3.9 MPa for a reaction temperature of 573 K. Here, DMDS was added to the feedstock (30 wt% tetralin and 70 wt% *n*-hexadecane), resulting in a sulfur concentration of 680 ppm. In these reactions, tetralin was converted into *trans*-decalin and *cis*-decalin, and its selectivity to decalins was almost 100%. After a time on stream of 70 h, the WHSV value returned to 4 h^{-1} and the tetralin conversion approached its initial level corresponding to this WHSV level. This recovery indicates

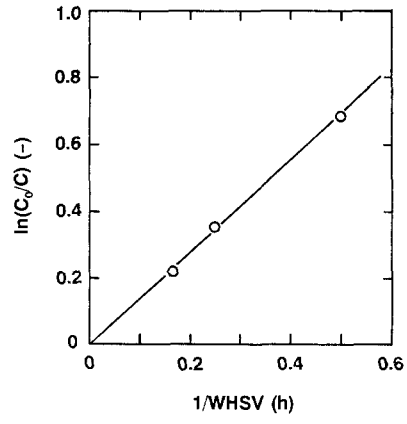

Fig. 2. Confirmation of first-order kinetics of tetralin hydrogenation.

that this run had little catalyst deactivation. Runs were also carried out for the NiMo catalysts with various amounts of added DMDS.

Fig. 2 shows the relationship between the $\ln(C_0/C)$ values and the 1/WHSV values for the sulfided (673 K) NiW catalyst, where C_0 and C indicate the tetralin concentration in the feedstock and product, respectively. This linear relationship indicates that the kinetics of the tetralin hydrogenation were first order in total tetralin content [6]. We therefore used a first-order rate constant k_{HYG} (h^{-1}) to evaluate the HYG activity of the NiW and NiMo catalysts in continuous-flow runs.

3.2. Effect of $P(H_2S)$ on HYG activity (continuous-flow runs)

Fig. 3 shows the effect of $P(H_2S)$ on the HYG activity of the sulfided (673 K) NiW and NiMo catalysts. Here, the x-axis is the measured $P(H_2S)/P(H_2)$. Both catalysts showed maximal HYG activity around a $P(H_2S)/P(H_2)$ of $3–5\times10^{-4}$. The steeper drop in HYG for the NiMo catalyst when $P(H_2S)/P(H_2)$ was below this level which indicated that this catalyst was much more sensitive to the $P(H_2S)$ level under the reducing conditions studied here. This sensitivity may be related to the structural changes of the active phase and will be discussed in Sections 3.5 and 3.6. The steeper drop in HYG activity for the NiW catalyst when $P(H_2S)/P(H_2)$ was higher than that for maximal HYG activity indicates that this catalyst was more sensitive to the inhibitory effect of H_2S adsorption on the active sites, as previously reported [7,8,9–12]. The reason for this difference in the inhibitory effect of H_2S between the two catalysts will be discussed in Section 3.4. In summary, the NiW catalyst was superior to the NiMo catalyst when $P(H_2S)/P(H_2)$ was below 3×10^{-3}, but inferior when $P(H_2S)/P(H_2)$ was above 3×10^{-3}. This figure shows that the NiMo catalyst is advantageous in the hydrogenation of high-sulfur feedstocks [3].

3.3. Hydrogenation over partially reduced, sulfided NiW and NiMo catalysts (batch runs)

Fig. 4 shows the relationship between the conversion of tetralin and the reduction temperature of the sulfided (673 K) NiW and NiMo catalysts. The left y-axis is the HYG activity over the non-reduced sulfided catalyst, and the right is the sulfur content of the partially reduced, sulfided catalysts before using in the hydrogenation tests. For the NiW catalyst, the HYG activity increased with increasing reduction temperature, and reached a maximum around 680 K. For the NiW catalyst sulfided at 773 K, which

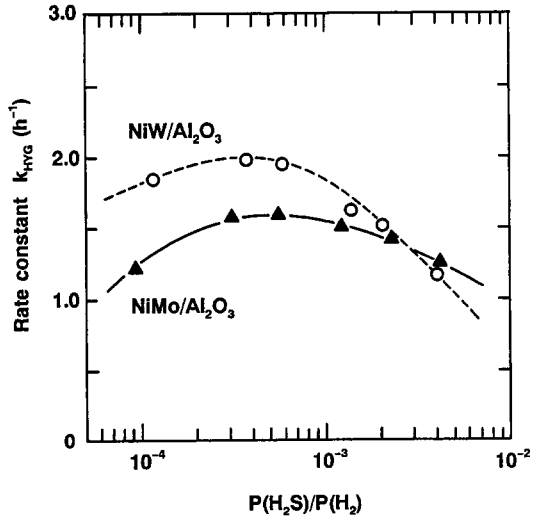

Fig. 3. Effect of H_2S partial pressure $P(H_2S)$ on hydrogenation activity of NiMo and NiW/Al_2O_3 catalysts. The x-axis shows the measured $P(H_2S)/P(H_2)$.

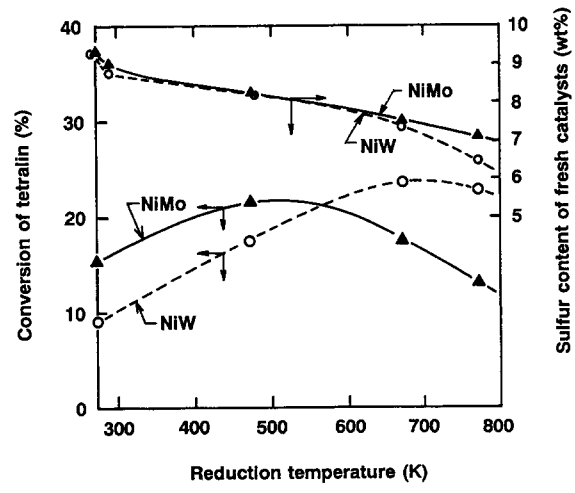

Fig. 4. Effect of reduction temperature on hydrogenation activity of sulfided catalysts and on the amount of sulfur of the fresh sulfided–reduced catalysts.

had a higher degree of sulfidation than the catalyst at 673 K, quite a similar tendency was observed: the HYG activities(conversion of tetralin) were 8.5, 18.5, 24.0, 27.0, and 24.0% for the sulfided catalysts which were non-reduced, reduced at 473 K, 573 K, 673 K, and 773 K, respectively, and the maximum HYG activity also occurred around 680 K. The NiMo catalyst showed a similar tendency, but the reduction temperature for the maximal HYG activity was around 500 K, which was quite lower than that for the NiW catalyst. For the reaction conditions where the non-reduced sulfided catalysts were used, the $P(H_2S)/P(H_2)$ values were quite high due to the H_2S removed from the sulfided catalysts. Using the data of the residual amount of sulfur after reduction at 573 K (reaction temperature for hydrogenating tetralin), we calculated a $P(H_2S)/P(H_2)$ value of about 3×10^{-3} for both the NiW and NiMo catalysts. Under this high $P(H_2S)$ condition, the NiMo catalyst was superior to the NiW catalysts under high $P(H_2S)$. However, when the reduction temperature exceeded 570 K, the NiW catalyst was superior.

If the high $P(H_2S)$ and low $P(H_2S)$ in Fig. 4 correspond to low and high reduction temperature regions, respectively, then the effect of $P(H_2S)/P(H_2)$ on HYG activity shown in Fig. 3 is clearly reproduced in Fig. 4.

When $P(H_2S)$ was high, both the NiW and NiMo catalysts were inhibited by H_2S (Fig. 3). This inhibitory effect of H_2S was more significant for the NiW catalyst than for the NiMo catalyst. This difference will be discussed in Section 3.4. When $P(H_2S)$ was low, both the NiW and NiMo catalysts were exposed to a sulfur-deficient atmosphere, where the sulfidic phases needed H_2S to maintain their sulfidic conditions. The resulting shortage of H_2S may have caused structural changes in the active phases.

For clarifying the effect of H_2S on the structural change of the active sulfidic phases in a H_2S deficient atmosphere, for convenience we characterized the sulfided–reduced catalysts rather than the spent catalysts used in the continuous-flow runs.

3.4. TPR analysis of sulfided catalysts

Fig. 5 shows the H_2S formation profiles during TPR of the sulfided (673 K) NiW (curve 2), sulfided NiMo (curve 3), W/Al_2O_3 (curve 1), Mo/Al_2O_3 (curve 5),

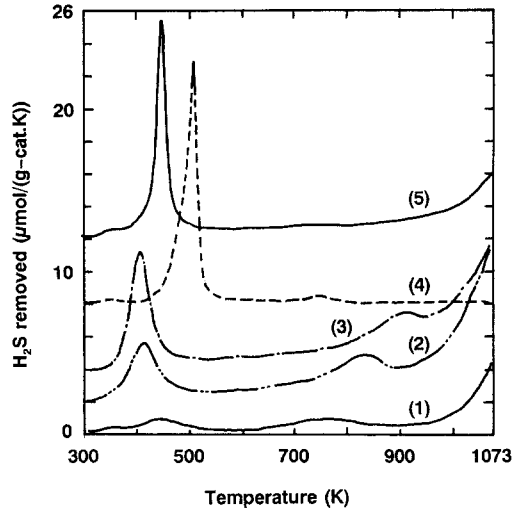

Fig. 5. Profiles of hydrogen sulfide formation during TPR of the sulfided catalysts: (1) W/Al_2O_3, (2) NiW/Al_2O_3, (3) $NiMo/Al_2O_3$, (4)Ni/Al_2O_3, and (5) Mo/Al_2O_3.

and Ni/Al_2O_3(curve 4) catalysts. For the Mo catalyst, the primary H_2S peak appeared at 443 K, and H_2S removal was significant above 983 K. Although the W catalyst showed a similar pattern, the amount of removed H_2S was quite low compared with that for the Mo catalyst; the secondary peak occurred at 750 K, and the amount of removed H_2S was significant above 963 K. The Ni catalyst showed two peaks: a primary peak at 503 K and a secondary one at 743 K. The NiMo and NiW catalysts both had two H_2S peaks and significant H_2S removal at high temperature.

For convenience, we divided the H_2S formation patterns into three temperature regions: <500 K (Region I); 500–900 K (Region II); and 900–1073 K (Region III). The primary H_2S peaks (Region I) originate mainly from the hydrogenation of the chemisorbed sulfur on the catalysts [13]. The peaks in Region II for both the NiW and NiMo catalysts originate from the H_2S released from the dispersed Ni–W(Mo)–S and Ni_3S_2 phases [13]. The H_2S formation in Region III for both the NiW and NiMo catalysts is from the H_2S released from the bulk WS_2-like crystallites and MoS_2-like crystallites phases, respectively.

Table 1 lists the amounts of sulfur removed in Regions I, II, and III for the NiW and NiMo catalysts (TPR data). The values in parentheses are the ratio of

Table 1
Amount of sulfur removed during TPR experiments

Catalysts	Sulfur removed (μmol/g)		
	Region I[a]	Region II[b]	Region III[c]
NiW/Al_2O_3	286	580	770
	(9.8%)	(19.8%)	(26.4%)
$NiMo/Al_2O_3$	392	538	760
	(13.4%)	(18.4%)	(26.0%)

[a] Region I—temperature region of T<500 K.
[b] Region II—temperature region of 500 K<T<900 K.
[c] Region III—temperature region of 900 K<T<1073 K.
[d] Value in parentheses indicated percentage of reduction of sulfur based on the total sulfur measured: Sulfur in NiW/Al_2O_3 catalyst=2922 μmol/g (i.e., 9.35 wt% S); Sulfur in $NiMo/Al_2O_3$ catalyst=2925 μmol/g (i.e., 9.36 wt% S).

sulfur removed as H_2S to the total amount of sulfur. Sulfur removal in Regions II and III was slightly higher for the NiW catalyst than that for the NiMo catalyst. The higher H_2S removal in Region II, where sulfur removal might be linked with the formation of the coordinatively unsaturated sites (CUS), for the NiW catalyst than for the NiMo catalyst may be related to the higher HYG activity for the NiW catalyst.

According to thermodynamical analyses [14], the metal–sulfur affinity in the bulk phases in decreasing order is Mo–S>W–S>Ni–S. This order reflects the increasing difficulty in reducing the sulfides, namely, Ni_3S_2>WS_2>MoS_2. Therefore, the potential to create CUS was higher for the NiW catalysts than for the NiMo catalysts, assuming that dispersion of active phases was similar. High reduction would cause formation of CUS ensembles on the sulfide phases, which in turn would cause formation of metallic phases. These thermodynamic results support the order in the reducibility of the bulk phases seen in our TPR experiments: Ni_3S_2>>WS_2> MoS_2.

Reducing properties of the CUS which appeared on the sulfide phases might influence the inhibitory effect of H_2S. The heat of sulfur adsorption on metal phases is generally 20–40% higher than the heat of formation of bulk sulfides [15,16]. This means that sulfur removal from the bulk sulfides studied here was much easier than that from metals on which sulfur was chemisorbed. Benard et al. [16] reported that the bond strength of sulfur on metals for Ni is higher than that for Mo. (Unfortunately, no data are available for W metal.) This means that Ni metallic phase was quite easily poisoned by H_2S adsorption. Therefore, the higher inhibitory effect of H_2S on the NiW catalyst than on the NiMo catalyst suggests that the CUS in the Ni–W–S phases were reduced to a greater extent than were the Ni–Mo–S phases.

H_2S removal was related not only to the formation of the CUS but also to the structural changes of the sulfide phases. To clarify these structural changes, we did an XPS analysis of the sulfided–reduced catalysts.

3.5. *XPS analyses of the sulfided–reduced catalysts*

Fig. 6(a) and (b) show the W 4f and Ni 2p spectra, respectively, for NiW catalysts first sulfided at 773 K (curve 1) and then reduced at 473 K (curve 2), 673 K (curve 3), and 773 K (curve 4). Tungsten oxide was difficult to be sulfided [17], and the $W^{4+}/(W^{4+}+W^{6+})$ values were 66% and 81% after the sulfidation at 673 K and 773 K, respectively. As mentioned in Section 3.3, the sulfidation temperature showed no significant influence on the relationship between the HYG activity and the reduction temperature of the sulfided NiW catalyst. Therefore, for comparing the sulfide phases of NiW catalyst with that of NiMo catalyst in the same degree of sulfidation, we characterized the NiW catalyst sulfided at 773 K instead of the NiW catalyst sulfided at 673 K. During reduction, no significant changes were observed for the W 4f spectra, implying that the WS_2-like sulfided phase was quite stable up to 773 K. On the other hand, both the sulfide (Ni_3S_2) and Ni^{2+} phases were present in the sulfided catalyst (curve 1 in Fig. 6(b)). As the reduction temperature was increased, the Ni sulfide phase was still dominant, but the peak height for the Ni^{2+} phase slightly increased.

Fig. 7(a) and (b) show the Mo 3d and Ni 2p spectra, respectively, for NiMo catalysts first sulfided at 673 K (curve 1) and then reduced at 473 K (curve 2) and 673 K(curve 3). (Note that the data for a reduction temperature of 773 K were corrupted due to a charging problem during the XPS measurements, and were therefore omitted from this figure.) The sulfided catalyst (curve 1) showed Mo^{4+}, Mo^{6+}, and S 2s peaks, and the degree of sulfidation was higher for MoO_3 (i.e., $Mo^{4+}/(Mo^{4+}+Mo^{6+})$=87%) in this sulfided catalyst than that for WO_3 in the NiW catalysts (66%).

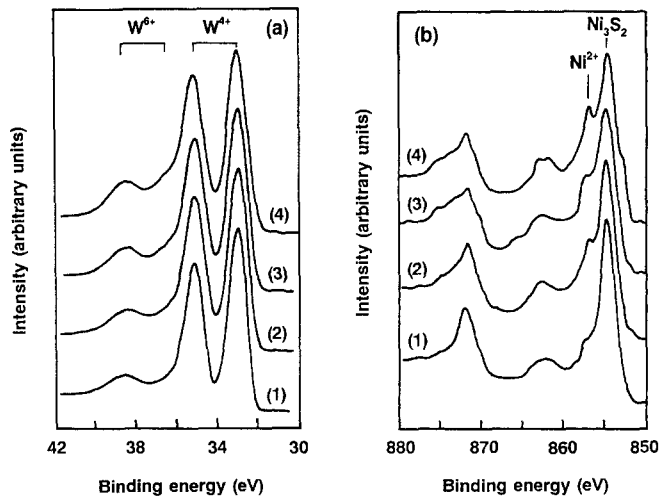

Fig. 6. Changes in XPS spectra of W 4f (a) and Ni 2p (b) for the NiW/Al_2O_3 catalysts during TPR: (1) sulfided at 773 K, (2) reduced at 473 K, (3) reduced at 673 K, and (4) reduced at 773 K.

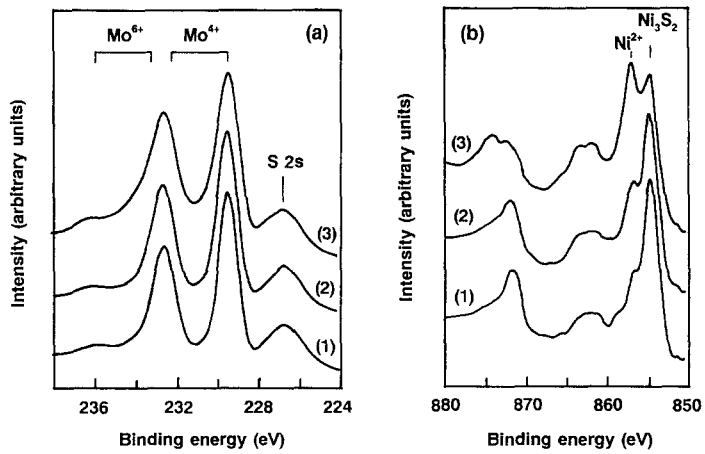

Fig. 7. Changes in XPS spectra of Mo 3d (a) and Ni 2p (b) for the $NiMo/Al_2O_3$ catalysts during TPR: (1) sulfided at 673 K, (2) reduced at 473 K, and (3) reduced at 673 K.

During reduction, no significant changes were observed for the Mo 3d spectra. On the other hand, the Ni 2p spectra underwent significant changes as shown in Fig. 7(b). After sulfidation, Ni sulfide phases were dominant, which is a pattern also seen in the NiW catalyst (Fig. 6(b)). After reduction at 673 K (curve 3), the Ni^{2+} became the dominant phase. The absence of sulfate peaks in the S 2p spectra of this catalyst suggests that the Ni^{2+} phases were caused by the formation of NiO or $NiAl_2O_4$ (spinel) phases. Table 2 shows the surface properties of the sulfided–reduced catalysts (sulfided at 773 K) from XPS measurements. The NiW catalyst showed no significant changes in the surface composition of the active phases up to a reduction temperature of 673 K. After the reduction at 773 K, the Ni concentration slightly decreased. For the sulfided (673 K) NiMo catalyst, the surface Mo and Ni concentrations did not change significantly

Table 2
Surface compositions of sulfided–reduced catalysts (XPS data)

Catalysts	Relative intensity in atomic ratio to Al				
	Mo 3d(W 4f) (%)	Ni 2p (%)	Al 2s (%)	S 2p (%)	Ni/W(Mo) (–)
NiW/Al_2O_3					
S	12.1	4.5	100	25.2	0.37
S–R(473 K)	12.3	4.2	100	23.5	0.34
S–R(673 K)	12.1	4.4	100	22.1	0.37
S–R(773 K)	12.1	3.3	100	21.6	0.28
$NiMo/Al_2O_3$					
S	10.3	4.4	100	20.1	0.43
S–R(473 K)	10.1	4.7	100	19.3	0.47
S–R(673 K)	10.1	4.2	100	16.5	0.41

S:sulfided, R:reduced under H_2 flow.

after reduction at 673 K, whereas the sulfur concentration significantly decreased. These changes in the surface compositions indicate that structural changes of the NiMo catalyst were accompanied by the removal of sulfur.

These XPS data indicate that the Ni and W sulfide phases on the NiW catalysts were quite stable during the reduction at temperatures up to 773 K. Therefore, H_2S removed during the TPR runs were mainly accompanied by the formation of CUS on the stable sulfide phases. On the contrary, structural changes during the reduction (at 673 K) of the NiMo catalysts occurred mainly in the Ni phase. Therefore, H_2S removed during the TPR runs, particularly in Region II, was accompanied by structural changes to the Ni phase, probably to the Ni–Mo–S and Ni_3S_2 phases.

For analyzing the structural changes of the active phases in more detail, we used EXAFS analysis.

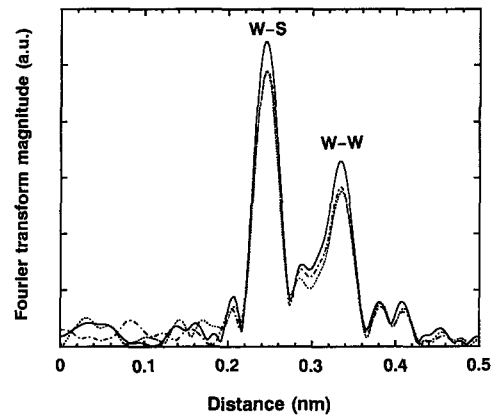

Fig. 8. Fourier transforms of W EXAFS spectra for the NiW/Al_2O_3 catalyst (k^3-weighed, Δk=14.0(3.5<k<17.5 Å^{-1}): fresh sulfided at 773 K (———), reduced at 623 K (— - —), and reduced at 773 K (- - -).

3.6. *EXAFS analysis of the sulfided–reduced catalysts*

Fig. 8 shows the Fourier transforms of the EXAFS spectra (W L_{III}-edge) for the NiW sulfided at 773 K (curve 1) and then reduced at 623 K (curve 2) and at 773 K (curve 3). All three catalysts showed two main peaks, at 0.241 nm and 0.315 nm, which correspond to the first W–S and W–W coordinations in WS_2 crystallites [5,18], respectively. The intensity of both peaks slightly decreased after reduction at 623 K, suggesting a slight decrease in the size of the (002) planes of the WS_2-like crystallites. However, further reduction at 773 K produced almost no change in the intensity of either peak, thereby implying no growth of the (002) planes between the temperature of 623 K and 773 K. These EXAFS results suggest that no sintering would occur for the WS_2-like phase on the NiW catalyst even under severe reducing conditions.

Fig. 9 shows the Fourier transforms of the EXAFS spectra (Mo K-edge) for the NiMo catalysts first sulfided at 673 K (curve 1), and then reduced at 623 K (curve 2) and at 773 K (curve 3). All three catalysts showed two main peaks, at 0.241 nm and 0.315 nm, which correspond to the first Mo–S and Mo–Mo coordinations in MoS_2 crystallites [5],

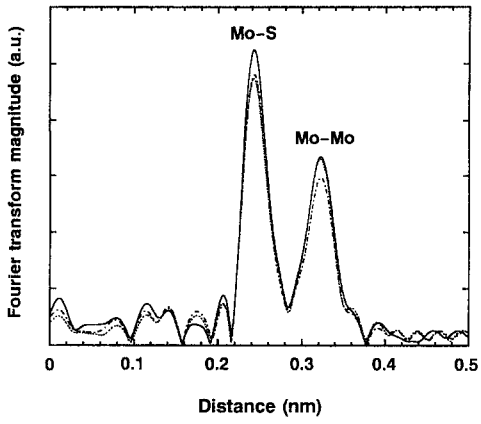

Fig. 9. Fourier transforms of Mo EXAFS spectra for the NiMo/Al_2O_3 catalyst (k^3-weighed, Δk=14.0(3.15<k<17.15 Å^{-1}): fresh sulfided at 673 K (———), reduced at 623 K (— — —), and reduced at 773 K (- - -).

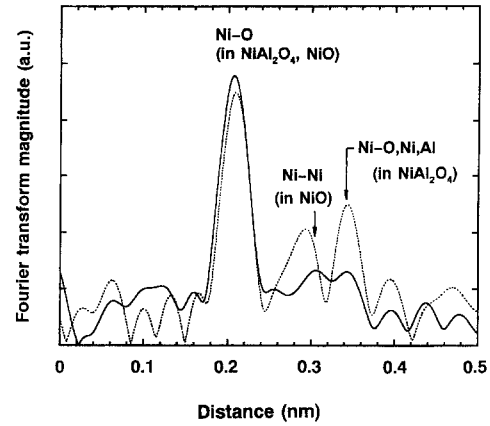

Fig. 10. Fourier transforms of Ni EXAFS spectra for the standard $NiAl_2O_4$ and calcined Ni/Al_2O_3 catalyst (k^3-weighed, Δk =10.0 (3.4<k<13.4 Å^{-1}): $NiAl_2O_4$ (- - -), and Ni/Al_2O_3 catalyst (———).

respectively. The intensity of both peaks slightly decreased after reduction at 623 K, suggesting a slight decrease in the size of the (002) planes of the MoS_2-like crystallites. However, after further reduction at 773 K, the intensity of the Mo–Mo peak increased, whereas that of the Mo–S peak slightly decreased. This indicates the growth of the (002) planes of MoS_2-like crystallites, namely, lateral sintering of MoS_2-like crystallites. Therefore, when we consider these results along with the XPS data, we conclude that MoS_2 phase sintering on the NiMo catalysts would start around 673 K under the reducing atmosphere.

Table 3 shows the melting points for the sulfides (bulk phase) studied here [19]. Unfortunately, no diffusion data are available for these compounds. Low melting points for the Ni sulfides after the formation of eutectic compounds suggest the ease of structural change for the Ni phases. The lower melting points for the MoS_2 phases than for the WS_2 phases after the formation of eutectic compounds suggest that the MoS_2 phase would more easily sinter than the WS_2 phase [20].

Table 3
Melting points of Ni, Mo and W compounds

Compound	Type	Temperature (K)
Ni	Melting	1728
Ni_3S_2(+Ni)	Eutectic	910
Ni_3S_2	Melting	1073
Mo	Melting	2896
MoS_2	Melting	2023±50
MoS_2(+Mo_2S_3)	Eutectic	1893
W	Melting	3695
WS_2	Melting	>2073
S	Melting	388

Fig. 10 shows the Fourier transforms of the EXAFS spectra (Ni K-edge) for the standard $NiAl_2O_4$ powder and calcined Ni/Al_2O_3 catalyst. The $NiAl_2O_4$ powder had two main peaks, at 2.07 nm and 0.343 nm. The first peak corresponds to the first Ni–O coordination of $NiAl_2O_4$, and the second peak corresponds to the second Ni–O coordination and to the first Ni–Ni and Ni–Al coordinations in $NiAl_2O_4$. The standard NiO powder (not shown in Fig. 10) had three main peaks, at 0.210 nm, 0.302 nm, and 0.415 nm, which correspond to the first Ni–O, first Ni–Ni, and second Ni–Ni coordinations in NiO crystallites, respectively. The Ni catalyst had three main peaks, at 0.207 nm, 0.306 nm, and 0.343 nm. The first peak might correspond to the Ni–O coordination in octahedral sites of $NiAl_2O_4$ (spinel) and the Ni–O coordination in NiO crystallites [21]. The second peak corresponds to the first Ni–O coordination in NiO crystallites. The third peak corresponds to the Ni–O, Ni–Ni, and Ni–Al coordinations in the $NiAl_2O_4$, which indicate the existence of $NiAl_2O_4$ phase in the calcined Ni catalyst.

Fig. 11 shows the Fourier transform of the EXAFS spectra (Ni K-edge) for the NiMo catalysts sulfided at

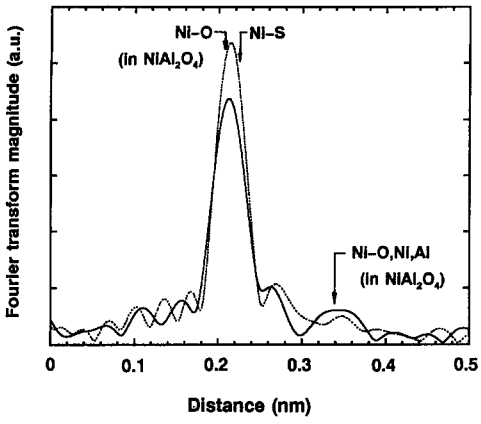

Fig. 11. Fourier transforms of Ni EXAFS spectra for the NiMo/Al_2O_3 catalyst (k^3-weighed, Δk=10.0(3.4<k<13.4 A^{-1}): sulfided at 673 K(- - -), and reduced at 723 K(———).

673 K and then reduced at 723 K. Both catalysts had a main peak at 0.213 nm, which might correspond to the Ni–O coordination in $NiAl_2O_4$ (0.208 nm) and the Ni–S coordination in Ni_3S_2 (0.225 nm) [18]. The peak intensity at 0.343 nm, which corresponds to the bonds in $NiAl_2O_4$, slightly increased after the sulfided catalyst underwent reduction. The bond distance obtained from the main peak slightly shortened after the reduction of the sulfided NiMo catalyst. This EXAFS data clearly indicates that the Ni^{2+} peak (in the XPS spectra) observed after reduction of the sulfided catalyst at 673 K was caused by the formation of the $NiAl_2O_4$ phases. Thermodynamical analyses of the formation of $NiAl_2O_4$ phases under reducing conditions will be reported in a subsequent paper.

The characterization data presented here indicate that stability of the sulfided NiMo catalysts was lower than that of the sulfided NiW catalysts under severe reducing conditions. Lower stability was caused by the sintering of the MoS_2-like phase as well as by the migration of the Ni phase into γ-Al_2O_3 to form the $NiAl_2O_4$ spinel. These structural changes might be linked with the loss of the active Ni–Mo–S phases, and thereby causing a significant decrease in the HYG activity as shown in Fig. 4 (high temperature reducing region) and in Fig. 3 (low $P(H_2S)/P(H_2)$ regions). In other words, the NiW catalysts were quite stable under the reducing conditions studied here, and are promising candidates for deep hydrogenation of low-sulfur feedstocks.

4. Conclusions

We studied the catalytic performance and the structural stability of NiW and NiMo catalysts prepared using citric acid as a complexing agent. From the results, we conclude the following:

1. NiW/Al_2O_3 catalysts are highly active in hydrogenating tetralin under low $P(H_2S)$, but the inhibitory effect of H_2S is significant when $P(H_2S)/P(H_2)$ exceeds 3×10^{-4},
2. NiMo/Al_2O_3 catalysts are superior to the NiW catalysts in hydrogenating tetralin under high $P(H_2S)$, i.e., $P(H_2S)/P(H_2)>2\times10^{-3}$,
3. the order for the reducibility of the bulk sulfide phases on the catalysts (TPR data) agreed with that predicted by thermodynamic calculations, then the potential to create CUS was higher for the NiW catalysts than for the NiMo catalysts,
4. stability of the sulfided NiMo/Al_2O_3 catalysts under the reducing conditions studied here is lower than that of the sulfided NiW catalysts due to the structural changes of the active phases, such as the formation of $NiAl_2O_4$ phase and sintering of the MoS_2-like phases,
5. the superiority of the sulfided NiW/Al_2O_3 catalysts over the sulfided NiMo/Al_2O_3 catalysts was indicated in deep hydrogenation of low-sulfur feedstocks.

Acknowledgements

The EXAFS work was performed under the approval of the Photon Factory Program Advisory Committee.

References

[1] A. Nishijima, T. Kameoka, H. Yanase, T. Sato, Y. Yoshimura, H. Shimada, N. Matsubayashi, Proc. Int. Conf. Coal Sci. 1991, p.759.
[2] C. Gachet, M. Breysse, M. Catteno, T. Decamp, R. Frety, M. Lacroix, L. de Mourgues, J.L. Portefaix, M. Vrinat, J.C. Duchet, S. Housni, M. Lakhdar, M.J. Tilliette, J. Bachelier, D. Cornet, P. Engelhard, C. Gueguen, H. Toulhoat, Catal. Today 4 (1988) 7.
[3] B.H. Cooper, A. Stanislaus, P.N. Hannerup, Hydrocarbon Processing, 83, 1993,.

[4] Y. Yoshimura, T. Sato, H. Shimada, N. Matsubayashi, M. Imamura, A. Nishijima, M. Higo, S. Yoshitomi, Catal. Today 29 (1996) 221.
[5] Y. Yoshimura, T. Sato, H. Shimada, N. Matsubayashi, M. Imamura, A. Nishijima, S. Yoshitomi, T. Kameoka, H. Yanase, Energy and Fuels 8 (1994) 435.
[6] A. Stanislaus, B.H. Cooper, Catal. Rev.-Sci. Eng. 36(1) (1994) 75.
[7] A.V. Sapre, B.C. Gates, Ind. Eng. Chem. Process Des. Dev. 21 (1982) 86.
[8] D.H. Broderick, A.V. Sapre, B.C. Gates, H. Kwart, G.C.A. Schit, J. Catal. 73 (1982) 45.
[9] N. Marchal, S. Mignard, S. Kasztelan, Catal. Today 29 (1996) 203.
[10] S. Gültekin, S.A. Ali, C.N. Satterfield, Ind. Eng. Chem. Process Des. Dev. 23 (1984) 179.
[11] S. Kasztelan, D. Guillaume, Ind. Eng. Chem. Res. 33 (1994) 203.
[12] H. Topsøe, B.S. Clausen, F.E. Massoth, Hydrotreating Catalysis, Springer, Berlin, 1996, p. 128.
[13] P.J. Mangus, A. Bos, J.A. Moulijn, J. Catal. 146 (1994) 437.
[14] Soc. Calorim. Therm. Japan, Thermodynamic Database MALT2, Kagakugijutsusha, Tokyo, 1992.
[15] J. Oudar, Catal. Rev.-Sci. Eng. 22(2) (1980) 171.
[16] J. Bénard, J. Oudar, N. Barbouth, E. Margot, Y. Berthier, Surface Science 88 (1979) L35.
[17] M. Breysse, M. Cattenot, T. Decamp, R. Frety, C. Gachet, M. Lacroix, C. Leclercq, L. de Mourgues, J.L. Portefaix, M. Vrinat, M. Houari, L. Grimblot, S. Kasztelan, J.P. Bonnelle, S. Housni, J. Bachelier, J.C. Duchet, Catal. Today 4 (1988) 39.
[18] H. Shimada, N. Matsubayashi, T. Sato, Y. Yoshimura, M. Imamura, T. Kameoka, H. Yanase, A. Nishijima, Jpn. J. Appl. Phys., 32, Suppl. 32-2, 463 (1993).
[19] T.B. Massalski, H. Okamoto, P.R. Subramanian, L. Kacprzak (eds.), Binary Alloy Phase Diagram, 2 edn., ASM International, Vol. 3, 1990.
[20] R. Fréty, M. Breysse, M. Lacroix, M. Vrinat, Bull. Soc. Chim. Belg. 93(8)–9 (1984) 663.
[21] C.N.R. Rao, G.U. Kulkarni, G. Saukar, G.R. Rao, K.R. Kannan, in: M. Graziani, C.N.R. Rao (eds.), Advances in Catalyst Design, World Scientific, Singapore, 1991, p. 1.